

## Electronic Supplementary Information

### Oxygen insertion reactions within the 1-D channels of phases related to $\text{FeSb}_2\text{O}_4$ .

Benjamin P. de Laune,<sup>#</sup> Gregory J. Rees,<sup>§</sup> Mariana J. Whitaker,<sup>#</sup> Hien-Yoong Hah<sup>a,@</sup>, Charles E. Johnson<sup>a</sup>, Jacqueline A. Johnson<sup>a,@</sup>, Dennis E. Brown<sup>%</sup>, Matthew G. Tucker,<sup>‡</sup> Thomas C. Hansen<sup>†</sup>, Frank J. Berry,<sup>#</sup> John V. Hanna,<sup>§</sup> Colin Greaves<sup>#,\*</sup>

<sup>#</sup> School of Chemistry, University of Birmingham, Birmingham B15 2TT, UK

<sup>§</sup> Department of Physics, University of Warwick, Coventry CV4 7AL, UK

<sup>a</sup> Center for Laser Applications, University of Tennessee Space Institute, Tullahoma, TN 37388, USA

<sup>@</sup> Department of Mechanical, Aeronautical and Biomedical Engineering, University of Tennessee Space Institute, Tullahoma, TN 37388, USA

<sup>%</sup> Department of Physics, Northern Illinois University, DeKalb, IL 60115, USA

<sup>‡</sup> Oak Ridge National Laboratory, Oak Ridge, TN 37831, USA.

<sup>†</sup> Institut Laue Langevin, BP 156, F-38042 Grenoble 9, France.

\*Corresponding author (c.greaves@bham.ac.uk)

## **S1. Full Experimental Details**

### **S1.1 Synthesis and thermal characterisation**

A variety of compounds with the schafarzikite structure were synthesised by heating intimately ground stoichiometric mixtures of dried metal oxides and metals (MgO,  $\geq 99\%$  325 mesh; Fe<sub>2</sub>O<sub>3</sub>,  $\geq 99.9\%$  Sigma-Aldrich; Sb<sub>2</sub>O<sub>3</sub>, Reagent Plus, Sigma Aldrich; CoO 325 mesh Sigma-Aldrich; Sb, BDH; PbO Reagent Plus 99.9+%) in evacuated sealed quartz tubes at 600-750°C for 6 hr periods with intermittent grinding. Alumina inserts were used to prevent reaction with the quartz. Oxidised phases were prepared by heating samples in air or oxygen. Thermogravimetric data were collected on a Netzsch Sta 449 F1 analyser under flowing oxygen at a rate of 10°C min<sup>-1</sup> to 800°C. For <sup>17</sup>O NMR analysis, samples of MgSb<sub>2</sub>O<sub>4</sub> and Sb<sub>2</sub>O<sub>3</sub> were exchanged with <sup>17</sup>O-enriched H<sub>2</sub>O hydrothermally and FeSb<sub>2</sub>O<sub>4</sub>-related phases were exchanged with <sup>17</sup>O-enriched oxygen gas (70% enrichment) at 350°C for times of 12-66 min. depending on the observed rate of oxygen absorption.

### **S1.2 Structural characterisation**

All X-Ray powder diffraction (XRPD) analysis was performed on a Bruker D8 diffractometer in transmission geometry: Cu-K<sub>α1</sub>, Lynxeye detector, Ge monochromator. Neutron powder diffraction (NPD) data for structure analysis were collected on the diffractometers HRPT at the Paul Scherrer Institut, Villigen, Switzerland and D20 at ILL, Grenoble, France. The high resolution diffractometer HRPT was used for detailed structural analysis on one sample contained in an 8 mm vanadium can at 300 K (calibrated wavelength 1.8852 Å). The high intensity D20 instrument (calibrated wavelength 1.5430 Å) was used for an *in situ* study on a sample held between porous quartz wool plugs in a 12 mm external diameter quartz tube. Data were continuously collected for intervals of 5 min while the sample was heated at 1°C min<sup>-1</sup> in oxygen to 500°C. Background data from an empty quartz tube were collected at

100°C intervals and were subtracted from each dataset such that the maximum temperature difference between the background and the sample collection temperature was 50°C. Crystal structures were refined by the Rietveld method<sup>1</sup> and the program "seqgsas" within the general structure analysis system, GSAS,<sup>2</sup> with the graphical user interface EXPGUI.<sup>3</sup>

Raman spectra were obtained using a Renishaw inVia Raman Microscope using laser radiation of wavelength 633 nm. Mössbauer spectra were recorded with a constant acceleration drive (SEECO, Edina, MN). The <sup>57</sup>Fe spectra were recorded at 298 K using a <sup>57</sup>Co/Rh source and a Kr proportional counter. <sup>121</sup>Sb spectra were collected at 298 K with a <sup>121m</sup>Sn source and a Xe proportional counter whilst those at 90 K were recorded in a Janis cryostat with a cooled Ge solid state detector. The <sup>121</sup>Sb spectra were fitted to a model where the broad Sb<sup>3+</sup> resonance reflected an unresolved electric quadrupole splitting. Velocity calibration was carried out with the <sup>57</sup>Co/Rh source and an iron foil absorber. All the isomer shift data are quoted relative to the centre of the iron spectrum.

### **S1.3 Solid state NMR and DFT calculations**

The <sup>17</sup>O MAS NMR data from diamagnetic MgSb<sub>2</sub>O<sub>4</sub> and Sb<sub>2</sub>O<sub>3</sub> were acquired at 20.0, 14.1, 11.7 and 7.05 T on a Bruker Avance III, Bruker Avance II+ 600, Bruker Avance III 500 and Varian Infinity+ 300 spectrometers operating at Larmor frequencies of 115.3, 81.3, 67.8 and 40.5 MHz, respectively. At each field a Bruker 3.2 mm HX MAS probe was employed to enable a rotational frequency ( $\nu_r$ ) of 20 kHz and deliver sufficient rf power for a 3  $\mu$ s  $\pi/2$  non-selective 'solution' pulse (i.e. 1  $\mu$ s  $\pi/2$  selective 'solid' pulse) for the spin  $I = 5/2$  <sup>17</sup>O quadrupolar nucleus. These measurements used a rotor-synchronised Hahn echo ( $\theta-\tau-2\theta-\tau$ ) sequence with a recycle delay of 5 s and a minimum of 40,000 transients were acquired at each field. All <sup>17</sup>O MAS NMR data were referenced to the primary H<sub>2</sub>O reference ( $\delta_{iso} = 0$

ppm),<sup>4</sup> which was also used to calibrate the <sup>17</sup>O pulse times. Two dimensional <sup>17</sup>O triple quantum MAS (2D 3QMAS) measurements were undertaken at 14.1 T using a Bruker Avance II+-600 spectrometer and a Bruker HX 3.2 mm probe which delivered an MAS frequency of 20 kHz. 3QMAS data were acquired using a three pulse Z-filter pulse experiment which consisted of a ‘non-selective’  $3\pi/2$  excitation pulse of 5.0  $\mu$ s duration, a  $\pi/2$  conversion pulse of 1.5  $\mu$ s duration, and followed by two ‘selective’  $\pi/2$  pulses of 15.0  $\mu$ s each which comprised the Z-filter.

The <sup>17</sup>O MAS NMR data from the oxidised paramagnetic materials (b)  $\text{Co}_{0.50}\text{Fe}_{0.50}\text{Sb}_2\text{O}_{4+y}$ , (c)  $\text{Co}_{0.25}\text{Fe}_{0.75}\text{Sb}_{1.75}\text{Pb}_{0.25}\text{O}_{4+y}$ , (d)  $\text{Mg}_{0.25}\text{Fe}_{0.75}\text{Sb}_{1.75}\text{Pb}_{0.25}\text{O}_{4+y}$  and (e)  $\text{Mg}_{0.50}\text{Fe}_{0.50}\text{Sb}_2\text{O}_{4+y}$  were undertaken at 7.05 T on a Bruker Avance III HD 300 spectrometer operating at a Larmor frequency of 40.5 MHz. A Bruker 3.2mm HX MAS probe was utilised to achieve a rotational frequency of 20 kHz, however further experiments were completed at 16 and 18 kHz to determine the true isotropic component of each paramagnetically broadened anisotropy. In a similar fashion to the measurements on the diamagnetic  $\text{MgSb}_2\text{O}_4$  system, all data were referenced to  $\text{H}_2\text{O}$  ( $\delta_{\text{iso}} = 0$  ppm)<sup>4</sup> and a similar pulse time characterisation was determined. All data were acquired using a rotor-synchronised Hahn echo ( $\theta-2\tau-2\theta-2\tau$ ) experiment with extended  $\tau$  delays to preserve all broad components within each spectrum. A 0.2 s recycle delay was determined as sufficiently slow to acquire unsaturated data, and a minimum of 700,000 transients were acquired for each sample. For each FID the full echo was acquired ensuring that no broad components were missed during acquisition.

Corresponding <sup>25</sup>Mg MAS NMR data from the  $\text{MgSb}_2\text{O}_4$  system were measured at 14.1 T using a Bruker Avance II+ 600 spectrometer which operated at the <sup>25</sup>Mg Larmor frequency of 36.7 MHz. A Bruker 3.2 mm HX probe enabled a MAS rotational frequency of 20 kHz and

delivered sufficient rf power for a  $9 \mu\text{s}$  ( $\pi/2$ ) non-selective ‘solution’ pulse (i.e.  $3 \mu\text{s}$   $\pi/2$  selective ‘solid’ pulse) for the spin  $I = 5/2$   $^{25}\text{Mg}$  quadrupolar nucleus. These measurements also used a rotor-synchronised Hahn echo ( $\theta-\tau-2\theta-\tau$ ) sequence with a recycle delay of 5 s. These data were referenced to the primary IUPAC 11M  $\text{MgCl}_{2(\text{aq})}$  reference ( $\delta_{\text{iso}} = 0$  ppm) via a secondary solid  $\text{MgO}$  reference ( $\delta_{\text{iso}} = 26$  ppm).<sup>4</sup>

All spectral simulations were completed using the Topspin SOLA fitting function. Estimates of the  $I = 5/2$   $^{17}\text{O}$   $\delta_{\text{iso}}$  and  $P_{\text{Q}}$  parameters were achieved by a graphical analysis of the variable  $B_0$  field data using the equation:

$$\delta_{\text{cg}} (\text{ppm}) = \delta_{\text{iso}} (\text{ppm}) - 3/500((P_{\text{Q}}^2/\nu_0^2) \times 10^6) \quad (1)$$

where  $\delta_{\text{cg}}$  is the  $B_0$  dependent second order quadrupole shift and  $P_{\text{Q}} = C_{\text{q}}(1+\eta_{\text{q}}^2/3)^{1/2}$  is the quadrupolar product.<sup>5</sup>

Density functional theory (DFT) calculations were performed to allow interpretation of the  $^{17}\text{O}$  spectra. All calculations used the CASTEP 8 code which employs Kohn-Sham DFT methodology using periodic plane-waves under the ultrasoft pseudopotential approximation.<sup>6</sup> The generalized gradient approximation for the exchange correlation energy was employed using the Perdew-Burke-Ernzerhof (PBE) functional.<sup>7</sup> The pseudopotentials were generated ‘on-the-fly’ using the standard Materials Studio pseudo-atom definitions (Accelrys, San Diego CA, USA).

The calculation was converged with respect to basis-set size and Brillouin zone k-point sampling to at least an accuracy of 0.4 mH ( $\sim 2 \times 10^{-6}$  % of total energy) per atom for each of the systems under investigation. To confirm this level of energy convergence was sufficient to produce accurate ionic forces, energy minimization with respect to ionic positions was

repeated with increasing plane wave cut off energy and density of k points within the Monkhorst-Pack Brillouin zone grid. This level of convergence was achieved using a plane wave cutoff energy of 800 eV for the systems, and by invoking k-point Monkhorst-Pack grids of  $3 \times 3 \times 3$ .

Geometry optimization calculations were performed on the systems using the over-converged values described previously to ensure accurate forces.<sup>8</sup> For these structural optimizations the lattice parameters were not fixed and the atomic positions were optimized to a force tolerance of 0.05 eV/Å, a maximum ionic displacement of  $1 \times 10^{-3}$  Å and a total energy change of  $2 \times 10^{-5}$  eV per atom. NMR parameter calculation of the chemical shift and electric field gradient tensors invoked the gauge included projector augmented-wave (GIPAW) DFT method which extended the pseudopotential (valence electron approximation) approximation to recover all electron charge densities. In order to calculate isotropic chemical shifts for each nucleus the relationship  $\delta_{\text{iso}} = -[\sigma - \sigma_{\text{ref}}]$  is invoked, where  $\sigma$  is the calculated isotropic shielding calculated against a bare atom and  $\sigma_{\text{ref}}$  is the reference isotropic shielding against a bare atom. This necessitated GIPAW DFT calculations be performed on two reference materials (MgO (<sup>25</sup>Mg) and Sb<sub>2</sub>O<sub>3</sub> (<sup>17</sup>O)).

#### **S1.4 Electronic conductivity**

Electronic conductivity data were collected from sintered pellets, typically 4 mm × 4 mm cross section and 15 – 30 mm long, using conventional 4-point contacts: silver wire attached with silver paint (Agar Electrodeag). Measurements were obtained from a Keithley 6220 DC current source linked directly to a Keithley 2182A nanovoltmeter and operating in Delta mode: a square-wave dc current is periodically reversed and the voltage averaged to remove any emf effects resulting from a temperature gradient between the voltage contacts.

Measurements were made in oxygen, nitrogen and air. Pellet densities varied between 50% and 80% of theoretical.

## S2 Results from XPS Measurements

Differentiation between the common oxidation states of antimony (Sb(V) and Sb(III)), and lead (Pb(IV) and Pb(II)) is difficult even for well-defined mixed-valent oxides such as  $\text{Sb}_2\text{O}_4$  and  $\text{Pb}_3\text{O}_4$  (see, for example, ref 9). Nevertheless, XPS spectra for all cations in  $\text{Co}_{0.25}\text{Fe}_{0.75}\text{Sb}_{1.75}\text{Pb}_{0.25}\text{O}_4$  and  $\text{Co}_{0.25}\text{Fe}_{0.75}\text{Sb}_{1.75}\text{Pb}_{0.25}\text{O}_{4+y}$  were obtained on a Kratos Axis Ultra DLD spectrometer and spectra are shown in Figures S3 – S6 with peak assignments. It was not possible to deduce reliable oxidation state data from the Sb, Pb and Fe spectra; the spectrum for Fe also provides a low signal:noise ratio. The spectrum for Co could not be observed even after data collection for 4 h. However, the XPS data provided no evidence to conflict with the much more reliable data obtained from  $^{57}\text{Fe}$  and  $^{121}\text{Sb}$  Mössbauer spectroscopy.

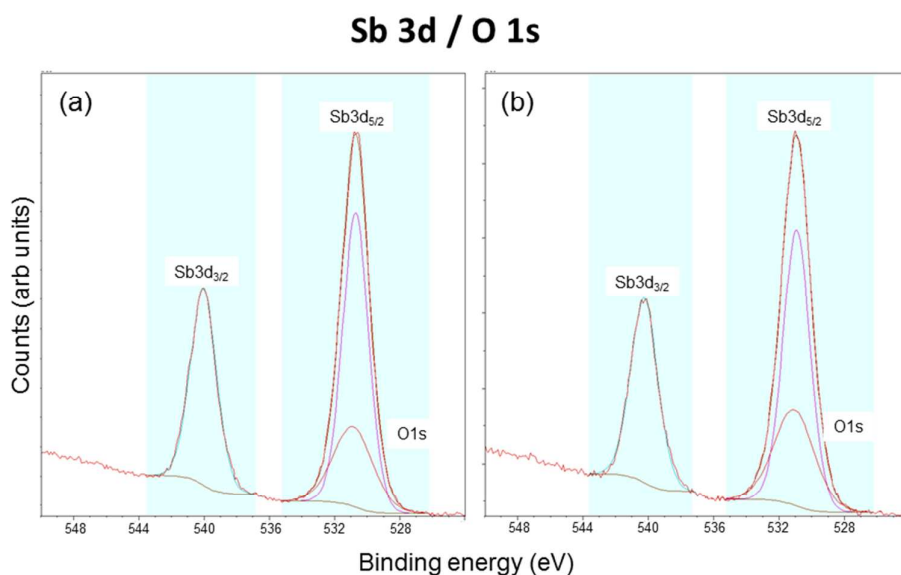


**Figure S1.** Sb3d XPS spectra from (a)  $\text{Co}_{0.25}\text{Fe}_{0.75}\text{Sb}_{1.75}\text{Pb}_{0.25}\text{O}_{4+y}$  and (b)  $\text{Co}_{0.25}\text{Fe}_{0.75}\text{Sb}_{1.75}\text{Pb}_{0.25}\text{O}_4$ .

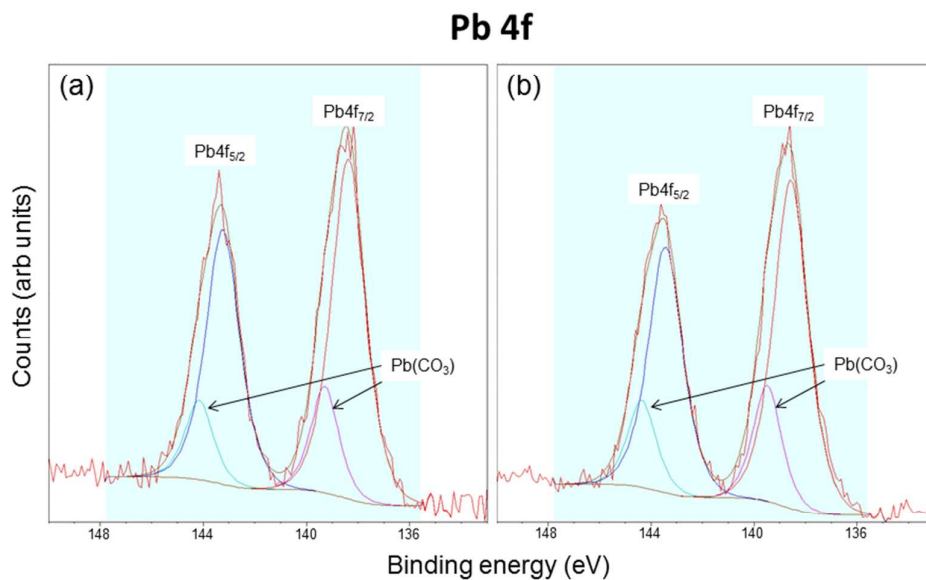


**Figure S2.** Pb4f XPS spectra from (a) Co<sub>0.25</sub>Fe<sub>0.75</sub>Sb<sub>1.75</sub>Pb<sub>0.25</sub>O<sub>4+y</sub> and (b) Co<sub>0.25</sub>Fe<sub>0.75</sub>Sb<sub>1.75</sub>Pb<sub>0.25</sub>O<sub>4</sub>. The tentative Pb(CO<sub>3</sub>) signals arise from surface contamination.

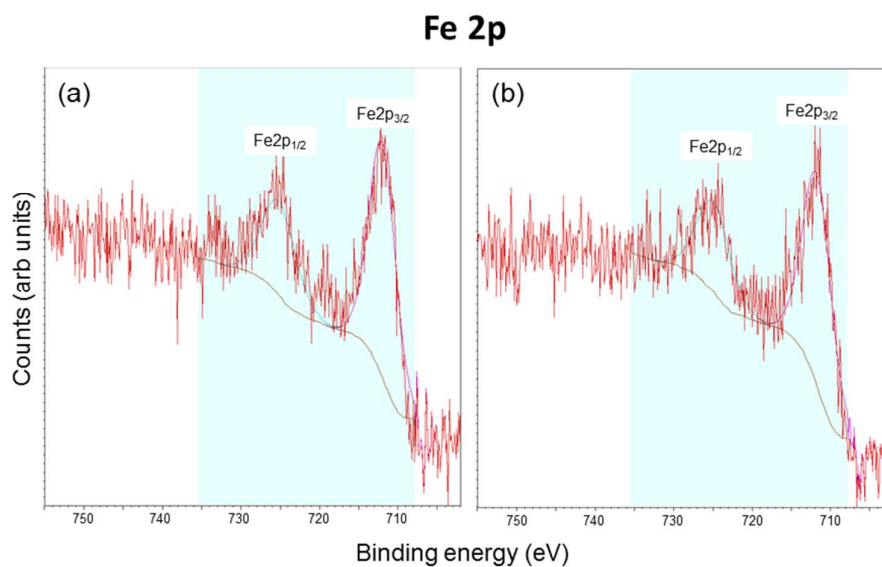


**Figure S3.** Fe2p XPS spectra from (a) Co<sub>0.25</sub>Fe<sub>0.75</sub>Sb<sub>1.75</sub>Pb<sub>0.25</sub>O<sub>4+y</sub> and (b) Co<sub>0.25</sub>Fe<sub>0.75</sub>Sb<sub>1.75</sub>Pb<sub>0.25</sub>O<sub>4</sub>.

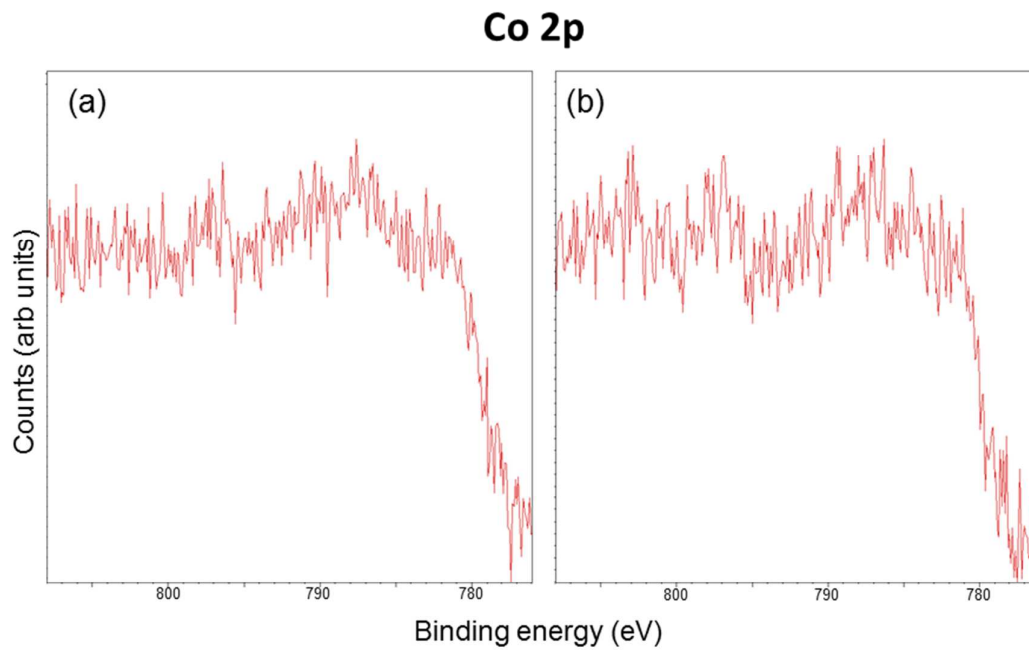


**Figure S4.** Co2p XPS spectra from (a)  $\text{Co}_{0.25}\text{Fe}_{0.75}\text{Sb}_{1.75}\text{Pb}_{0.25}\text{O}_{4+y}$  and (b)  $\text{Co}_{0.25}\text{Fe}_{0.75}\text{Sb}_{1.75}\text{Pb}_{0.25}\text{O}_4$ .

## References

- (1) Rietveld H. M. A profile refinement method for nuclear and magnetic structures. *J. Appl. Crystallogr.*, **1969**, *2*, 65-71.
- (2) Larson A. C.; Von Dreele R. B. General Structural Analysis System (GSAS). *Los Alamos National Laboratory LAUR 86-748*, **2004**.
- (3) Toby B. H. EXPGUI, a graphical user interface for GSAS. *J. Appl. Crystallogr.*, **2001**, *34*, 210-213.
- (4) Harris R. K.; Becker E. D.; Cabral de Menezes S. M.; Goodfellow R.; Granger P. NMR nomenclature: nuclear spin properties and conventions for chemical shifts. IUPAC Recommendations 2001. *Magn. Reson. Chem.*, **2002**, *40*, 489-505.
- (5) Samoson A.; Lippmaa E. Synchronized double-rotation nmr-spectroscopy. *J. Magn. Reson.*, **1989**, *84*, 410-416.
- (6) Clark S. J.; Segall M. D.; Pickard C. J.; Hasnip P. J.; Probert M. J.; Refson K.; Payne M. C. First principles methods using CASTEP. *Z Kristallogr.*, **2005**, *220*, 567-570.
- (7) (a) Perdew J. P.; Chevary J. A.; Vosko S. H.; Jackson K. A.; Pederson M. R.; Singh D. J.; Fiolhais C. Atoms, molecules, solids, and surfaces - applications of the generalized gradient approximation for exchange and correlation. *Phys. Rev. B*, **1992**, *46*, 6671-6687 (b) Perdew J. P.; Chevary J. A.; Vosko S. H.; Jackson K. A.; Pederson M. R.; Singh D. J.; Fiolhais C. Atoms, molecules, solids, and surfaces - applications of the generalized gradient approximation for exchange and correlation (vol 46, pg 6671, 1992). *Phys. Rev. B*, **1993**, *48*, 4978-4978.
- (8) Pickard C. J.; Mauri F. All-electron magnetic response with pseudopotentials: NMR chemical shifts. *Phys. Rev. B*, **2001**, *63*, 245101.
- (9) NIST X-ray Photoelectron Spectroscopy Database, Version 4.1 (National Institute of Standards and Technology, Gaithersburg, 2012); <http://srdata.nist.gov/xps/>.